Hunan Daxue Xuebao/Journal of Hunan University Natural Sciences
ISSN：1674-2974 | CN 43-1061 / N

DOI: 10.5281/zenodo.10450360
Vol: 60 | Issue: 12 | 2023

NUMERICAL SIMULATION OF PRESSURIZED FLUSHING AT DIFFERENT WATER LEVELS (CASE STUDY: SEFID-RUD DAM)

MOSTAFA ADINEH

PhD Candidate, Department of Civil Engineering, Kish International Branch, Islamic Azad University, Kish Island, Iran. E-mail: mostafa.adinehloo1980@yahoo.com

MAHMOOD SHAFAI BEJESTAN *

Professor, Department of Water and Environmental Engineering, Shahid Chamran University of Ahvaz, Ahvaz, Iran. *Corresponding Author E-mail: m-shafaeibejestan@scu.ac.ir

HESAM GHODOOSI

Assistant Professor, Department of Water Engineering, University of Zanjan, Iran.
E-mail: ghodousi_he@yahoo.com

Abstract

Pressurized hydraulic flushing is a technique to remove deposited sediments in reservoirs. Dam outlets are opened to discharge sediments through the outflow. Reservoirs cannot be experimentally simulated at a real-life scale under various scenarios. Therefore, numerical simulations represent an efficient and effective alternative and help optimally manage deposited sediments in reservoirs. This paper numerically simulated flow and sediments in the Sefid-rud Dam, Iran, using the Flow-3D model. The numerical model was calibrated using real-life flushing data of the dam. Then, the effects of the water level at the beginning of pressurized flushing and the number of open outlets were explored by analyzing the changes in the longitudinal bed level, scour around the outlets, and sediment removal. It was found that the numerical model was effective and efficient in identifying the optimal initial reservoir level and outflow in a dam.

Keywords: *Flushing, Dam, Numerical simulation, CFD, Sefid-rud Dam, Flow-3D*

INTRODUCTION

Today, reservoir sedimentation is the most important threat to the lifespan of dams. This is even more challenging in developing countries due to the inefficient management of basins. Reservoirs have a lifespan of 40-50 years in the world, and it is estimated that reservoirs undergo a lifespan decline of 0.5-1.0% every year due to sedimentation (Talebbeydokhti and Naghshineh 2004; Schleiss et al., 2016). The deposition of sediments not only reduces the reservoir capacity but also may disturb the functioning of mechanical components, e.g., turbines and floodgates. In general, reservoir flushing is classified into mechanical flushing and hydraulic flushing. The former removes sediments through mechanical techniques, such as dredging, while the latter discharges sediments through outflows, e.g., bypass channels, expelling the turbidity current, and flushing (Shen, 1999). Flushing is a frequently used sediment removal method. It is divided into drawdown flushing and pressurized flushing. Drawdown flushing removes sediments by completely draining the reservoir, while the water quantity remains almost unchanged in pressurized flushing (White, 2001). Research has shown that the former has higher performance (Morris and Fan, 2010; Madadi et al., 2016; Beyvazpour et al., 2021). However, the drainage of a reservoir imposes adverse environmental impacts downstream of the dam. Hence, pressurized flushing has been recommended for dams with relatively large reservoirs (Powell and Khan, 2012). The literature on the removal of sediments from reservoirs can be classified

ISSN：1674-2974 | CN 43-1061 / N

DOI: 10.5281/zenodo.10450360
Vol: 60 | Issue: 12 | 2023

into complete sediment removal (e.g., flushing), the removal of sediments around the bottom outlet via structures, and the prediction of sediment removal using artificial intelligence (AI).

Numerous numerical and experimental studies have been conducted on flushing. Shen (1999) investigated the sediment transport mechanism in drawdown flushing through an experimental model. Meshkati et al. (2009) reported an experimental study on scour cone development. Haun and Olsen (2012) developed a 3D numerical model to simulate the flushing of the Kali Gandaki Dam, Nepal. Castillo et al. (2015) two-dimensionally modeled the flushing of the Paute-Cardenillo Dam. Chaudhry et al. (2014) simulated flushing in the reservoir of the Baira Dam, India, using a numerical model. Power and Khan (2015) studied the velocity distribution downstream of an orifice with a rigid upstream bed using both experimental and numerical models. It was found that the velocity was larger below the orifice centreline than at the centreline. Iqbal et al. (2019) two-dimensionally simulated the sediment erosion level due to drawdown flushing. Although earlier works mostly modeled the reservoir level, a number of studies reported local modeling of flow pattern and structure effects on the flow pattern and erosion in the vicinity of the outlets. Melville (2008) found that barriers in front of the flow would create a low-pressure zone downstream of the barriers, creating wake vortices and transporting sediments in the barrier zone. Jenzer-Althaus et al. (2014) enhanced the diffusion of suspended sediments by inducing turbulence through a radial jet flow upstream of the orifice. Madadi et al. (2016) employed cylindrical piles upstream of the orifice and reported a 250% improvement in sediment removal. Madadi et al. (2017) increased the scour depth by 280% using a projecting semi-circular (PSC) structure. Haghjouei et al. (2021) reported a ten-fold rise in sediment removal using a bottomless structure upstream of the outlet. Beyvazpour et al. (2021) reported a seven-fold improvement in sediment removal via piles of a triangular cross-section upstream of the orifice. Naderi et al. (2022) experimentally and numerically studied the flow pattern around a sediment enhancement plane upstream of an orifice.

AI models have rarely been employed in flushing research. Emamgholizadeh et al. (2013) evaluated the flushing cone volume and length using an artificial neural network (ANN), the adaptive neuro-fuzzy inference system (ANFIS), and empirical data. They reported that the ANN and ANFIS models had high predictive power. Li et al. (2016) simulated flushing in the Three Gorges Dam, China, using an ANN model. They found that the ANN model was substantially effective in relating sediment removal prediction to influential parameters. Daryaee et al. (2022) used AI and data pre-processing to predict longitudinal and transverse pressure flushing cone profiles. Previous studies mostly implemented 1D and 2D simulations, and flushing has rarely been simulated three-dimensionally from hydraulic perspectives. Therefore, the present study simulated the flushing of the Sefid-rud Dam, Iran, using the Flow-3D model under different scenarios. To validate the numerical model, the results were compared to the data of a real-life flushing operation. Then, scenarios were defined to optimize the flushing parameters.

MATERIALS AND METHODS

Case study

This paper employed the Sefid-rud Dam as the case study. The Sefid-rud Dam is a buttress concrete dam located near Manjil, Guilan Province. It has a height of 106 and a crest length of 425 m and was constructed to store water for agricultural demands in the Guilan Plain, drink water demand, and power generation. The Sefid-rud Dam has three bottom outlets on the right side at a level of 191.3 m with a total discharge capacity of 430 m^3/s, as shown in Fig. 1. It has an elevation of 271.6 m from the sea level and a storage capacity of 1760×10^6 m^3. It underwent a 30% decline in the reservoir capacity in seventeen years of operation with a massive quantity of sediments (46 million tons per year) due to a lack of vegetation in the basin, seasonal rainfalls leading to heavy floods, and insisting on not

ISSN：1674-2974 | CN 43-1061 / N

DOI: 10.5281/zenodo.10450360
Vol: 60 | Issue: 12 | 2023

opening the bottom outlets under flood events to generate power. Figure 2 shows a photograph of the Sefid-rud Dam, in which the bottom outlet is completely buried, with a sediment front 300 m from the dam above the inlet elevation of the floodgates with a threshold elevation of 210.1 m. The sediment height is nearly 20-25 m based on the bed elevation of the bottom outlets (i.e., 191.30 m).

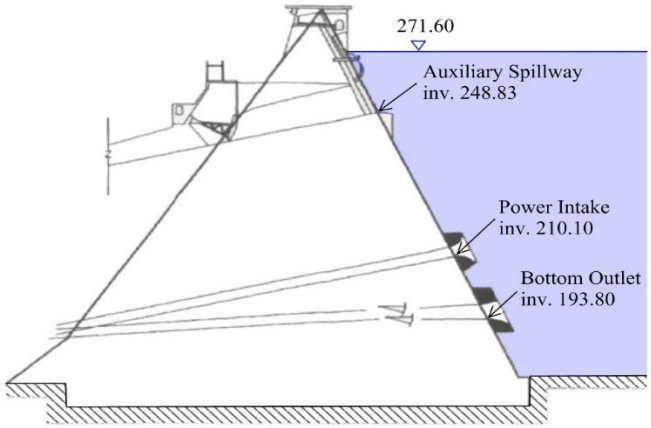

Figure 1: Placement of the bottom outlets and intakes of the Sefid-rud Dam

Figure 2: Sediments deposited in the reservoir of the Sefid-rud Dam

This study implemented simulations at two reservoir levels, including 234.6 m (at which the 2004 flushing was performed) and 271.6 m (normal dam elevation). Three scenarios were defined at each level. The scenarios included (I) draining water and sediments at the maximum discharge capacity (i.e., all five outlets opened), (II) opening the two left outlets with the three right outlets closed, and (III) opening the three right outlets with the two left outlets closed. A total of six flushing scenarios were implemented, comparing the results to the data of the 2004 flushing operation to identify the optimal flushing parameters based on the water level and the number of open outlets to maximize sediment removal and scour depth in the longitudinal profile.

Flow-3D model

Governing equations

This study exploited the Flow-3D model to three-dimensionally simulate the flow and sedimentation using the finite volume method (FVM). The governing equations included the conversation of mass and the conservation of momentum. The conservation of mass is written as (Flow-3D User Manual, V11, 2015):

ISSN：1674-2974 | CN 43-1061 / N

DOI: 10.5281/zenodo.10450360
Vol: 60 | Issue: 12 | 2023

$$V_F \frac{\partial(\rho)}{\partial t} + \frac{\partial}{\partial x}(uA_x) + \frac{\partial}{\partial y}(vA_y) + \frac{\partial}{\partial z}(wA_z) = \frac{R_{SOR}}{\rho} \quad (1)$$

which gives the incompressible form of the continuity equation, and *u, v,* and *w* denote the velocity components in the *x*-, *y*-, and *z*-directions, respectively, A_x, A_y, and A_z are the area fractions of the flow in the *x*-, *y*-, and *z*-directions, respectively, V_F is the volume fraction of the flow, ρ denotes density, and R_{SOR} denotes the source of mass. The momentum equation can be written as:

$$\begin{aligned}
&\frac{\partial u}{\partial t} + \frac{1}{V_F}\left(uA_x\frac{\partial u}{\partial x} + vA_y\frac{\partial u}{\partial y} + wA_z\frac{\partial u}{\partial z}\right) = -\frac{1}{\rho}\frac{\partial \rho}{\partial x} + G_x + f_x \\
&\frac{\partial v}{\partial t} + \frac{1}{V_F}\left(uA_x\frac{\partial v}{\partial x} + vA_y\frac{\partial v}{\partial y} + wA_z\frac{\partial v}{\partial z}\right) = -\frac{1}{\rho}\frac{\partial \rho}{\partial y} + G_y + f_y \\
&\frac{\partial w}{\partial t} + \frac{1}{V_F}\left(uA_x\frac{\partial w}{\partial x} + vA_y\frac{\partial w}{\partial y} + wA_z\frac{\partial w}{\partial z}\right) = -\frac{1}{\rho}\frac{\partial \rho}{\partial z} + G_z + f_z
\end{aligned} \quad (2)$$

Where G_x, G_y, and G_z are the body accelerations, while f_x, f_y, and f_z denote the viscosity-induced accelerations in the *x*-, *y*-, and *z*-directions, respectively (Fathi-Moghaddam et al., 2018).

This study evaluated the standard K-ε, RNG K-ε, and K-ω turbulence models in calibration. The RNG K-ε model was found to outperform the standard K-ε and K-ω models. Takhot and Orszag (1986) developed the RNG K-ε model as an augmented variant of the K-ε model, in which the coefficients are obtained from theoretical analysis rather than experimental data. It has higher compatibility than the K-ε model (Flow-3D User Manual, V11, 2015).

The bed load model was similar to that of Chen (2006) and ignores suspended sediments. This study used the drag-dependent bed load transport rate equation to evaluate the bed load. The flow drag τ, sediment transport threshold drag τ_c, Shields number θ, and critical Shields number θ_c are given by:

$$\tau = \rho U_*^2 \quad (3)$$

$$\tau_c = \rho U_{*c}^2 \quad (4)$$

$$\theta = \frac{\tau}{g(\rho_s - \rho)d} \quad (5)$$

$$\theta_c = \frac{\tau_c}{g(\rho_s - \rho)d} \quad (6)$$

where U_* is the shear velocity, U_{*c} is the critical shear velocity, ρ is the fluid density, ρ_s is the sand density, and d denotes the average sedimentary particle diameter. Engelund and Fredsoe (1976) formulated the bed load transport rate as:

$$q_b = \rho_s \frac{\pi}{6} d^3 \frac{1}{d^2} u_b p \quad (7)$$

where q_b is the bed load transport rate per unit width, u_b is the average bed load transport velocity, and p is the sedimentary particle movement probability. As can be seen, the bed load transport rate for a given particle is dependent only on u_b and p. The driving force of a single particle is calculated as:

$$F_D = C_D \frac{\pi}{4} d^2 \rho \frac{(aU_* - u_b)^2}{2} \quad (8)$$

ISSN：1674-2974 | CN 43-1061 / N

DOI: 10.5281/zenodo.10450360
Vol: 60 | Issue: 12 | 2023

The friction force is written as:

$$f_D = g(\rho_s - \rho)\frac{\pi}{6}d^3\beta \tag{9}$$

The driving force is equal to the friction force. Therefore,

$$\frac{u_b}{U_*} = a(1 - \sqrt{\frac{4\beta}{3a^2 C_D \theta}}) \tag{10}$$

Since $\theta_0 = \frac{4\beta}{3a^2 C_D}$,

$$\frac{u_b}{U_*} = a(1 - \sqrt{\frac{\theta_0}{\theta}}) \tag{11}$$

where C_D is the drag coefficient, while aU_* is the water velocity in the bed load movement area. In the vicinity of the bed, $a = 6 - 10$ when $u_b = 0$ and $\theta = \theta_0$. In other words, θ_0 is the relative drag force that prevents sediment movement. Therefore, θ_0 is smaller than the critical drag force θ_c, and Eq. (11) is rewritten as:

$$\frac{u_b}{U_*} = a(1 - 0.7\sqrt{\frac{\theta_0}{\theta}}) \tag{12}$$

The drag force is the total of the critical drag applied to the sand bed and the drag force applied to moving sedimentary particles:

$$\tau = \tau_c + ng(\rho_s - \rho)\frac{\pi}{6}d^3\beta \tag{13}$$

where *n* is the number of sedimentary particles. The number of sedimentary particles per unit area $\frac{1}{d^2}$ and the sand particle movement probability *p* are related as $p = n/\frac{1}{d^2}$. Based on Eqs. (5) and (6), *p* can be written as:

$$p = \frac{6}{\pi\beta}(\theta - \theta_c) \tag{14}$$

As mentioned, u_b and p are determinants of the bed load transport rate. The insertion of u_b and p from Eqs. (12) and (14) into Eq. (7) gives the bed load transport rate based on the dynamic friction coefficient $\beta = 0.8$ and constant $a = 9.3$ as:

$$q_b = \begin{cases} 11.6\rho_s d(\theta - \theta_c)\left(\sqrt{\theta} - 0.7\sqrt{\theta_c}\right), \theta \geq \theta_c \\ 0, \quad \theta < \theta_c \end{cases} \tag{15}$$

Which is employed in the present work. According to Eqs. (12), (14), and (15), the bed load model be calculated using the Shields number for given sediments. Erosion occurs at a location where the Shields number exceeds the critical Shields number on the bed.

Numerical setup

The numerical model, including the reservoir topography, dam position and size, outlets, and spillway, was developed in GIS and Civil 3D and imported as a *stl* file to Flow-3D. Table 1 reports the sedimentary particle parameters, including the diameter and fraction.

DOI: 10.5281/zenodo.10450360
Vol: 60 | Issue: 12 | 2023

Table 1: Distribution and parameters of sedimentary particles on the reservoir bed of the Sefid-rud Dam

Grain Size	d_{min} (mm)	d_{max} (mm)	d_{mean} (mm)	PEF %
D0-30	0.0025	0.0025	0.0025	30%
D30-50	0.0025	0.007	0.00475	20%
D50-60	0.007	0.0085	0.00775	10%
D60-90	0.0085	0.03	0.0192	30%
D90-100	0.03	0.065	0.0475	10%

To simulate the flushing operation, an area of the reservoir and the dam wall were modeled in the form of two mesh blocks, as shown in Fig 3(a). The dam wall, wall-adjacent area, and bottom outlets were in mesh block 1, while the remaining part of the domain was placed in mesh block 2. A larger number of cells were applied to mesh block 1 due to the velocity gradient to enhance model accuracy. The dam wall was assumed to be solid, while the bed of the reservoir was assumed to be sedimentary. Table 2 represents the mesh sizes of the two mesh blocks. Mesh block 1 had a length of 585 m and a width of 180, with a total of 336960 cells with a length of 5 m, a width of 5 m, and a height of 0.857 m. Mesh block 2, however, had a length of 980 m and a width of 585 m and involved 231280 meshes with a length of 10 m, a width of 9.93 m, and a height of 1.75 m. Figure 3(b) shows the boundary conditions of the two mesh blocks.

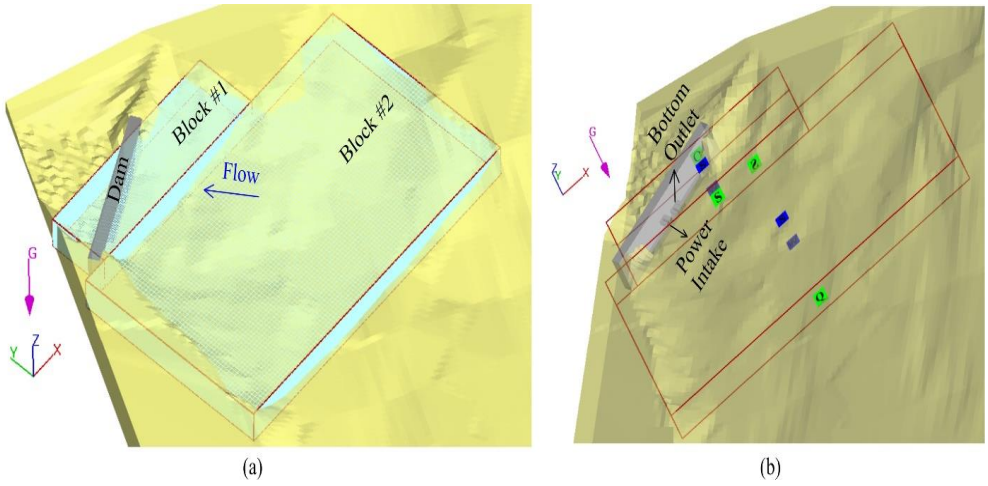

Figure 3: Representation of (a) mesh blocks and (b) boundary conditions

Table 2: Mesh parameters of mesh blocks 1 and 2

Parameter	Mesh Block #1			Mesh Block #2		
Direction	x	y	z	x	y	z
Number of cells	117	36	80	98	59	40
Maximum cell size (m)	5.01	5	0.87	10.02	9.93	1.75
Total cells	336960			231280		

Numerical model calibration

To calibrate numerical models to simulate erosion and sedimentation, either bed profile comparison or transported sediment concentration could be exploited. Long-term flushing calibration (several months) is typically carried out based on the former approach, while the latter is adopted for short-term flushing calibration (a few days or hours). Figure 4 compares the measured and simulated flushed sediment concentrations. As can be seen, the numerical model accurately simulated flushing.

ISSN：1674-2974 | CN 43-1061 / N

DOI: 10.5281/zenodo.10450360
Vol: 60 | Issue: 12 | 2023

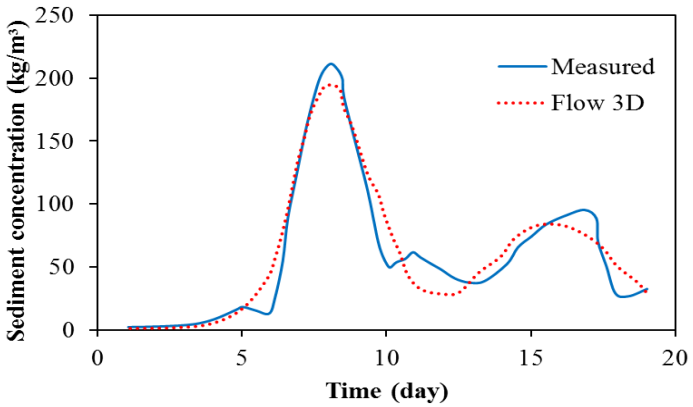

Figure 4: Empirical versus numerical sediment concentrations in Flow-3D

RESULTS AND DISCUSSION

The reservoir water level at the beginning of pressurized flushing and the discharge rate play key roles in flushing effectiveness. These two parameters are independent of ambient parameters and dependent on dam operation. The present study evaluated the effects of the initial reservoir level (by changing the reservoir level at the beginning of flushing) and discharge rate (by changing the number of open outlets). Figure 5(a) shows the reservoir, wall, and bottom outlets of the Sefid-rud Dam before the simulation. As can be seen, the sediment quantity near the dam wall was large enough to bury the three right outlets entirely and the left outlets partially. Figure 5(b) depicts the flushed dam wall and bottom outlets. As can be seen, a large fraction of sediments were discharged upon flushing, leading to a scour pit and removing sediments from the two left outlets entirely and from the three right outlets partially. It was found that the maximum flushing occurred in the form of a cone in the vicinity of the bottom outlets. The cone can be divided into two distinctive parts. The first part was a central cavity near the wall of the model along the bottom outlet arising from gravitational sediment discharge. The second part, however, was a slope with a smooth end stemming from the vertical movement of the flow toward the central cavity. Pressurized flushing was mostly concentrated on the areas around the outlets. To implement a flushing channel along the reservoir and remove a large quantity of sediments, a river stream is required, which is known as drawdown flushing.

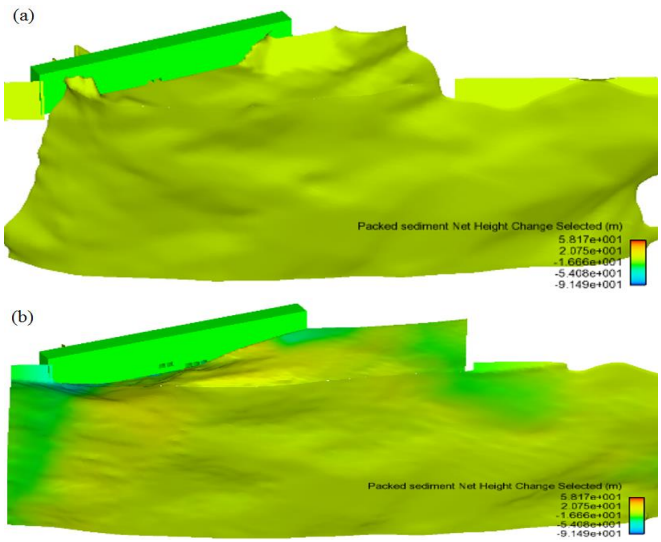

Figure 5: Topography of the non-flushed and flushed reservoir models

ISSN：1674-2974 | CN 43-1061 / N

DOI: 10.5281/zenodo.10450360
Vol: 60 | Issue: 12 | 2023

Figure 6 depicts the flushing outcome at a reservoir level of 234.6 m with two, three, and five open outlets. Figure 7 illustrates the flushing outcomes at a reservoir level of 271.6 m. As can be seen, a large quantity of sediments deposited at a distance of up to 600 m from the wall was removed. It was found that sediment removal at a reservoir level of 271.6 m was maximized when all five outlets were opened. Sediment removal at a reservoir level of 271.6 m with three and two open outlets was lower. It was observed that the opening of all five outlets was the first determinant of sediment removal at a given average inflow rate for both reservoir levels of 271.6 and 234.6 m, whereas the second determinant was the flushing time. The optimal flushing with the maximum sediment removal and maximum scour depth in the longitudinal reservoir profile occurred at a reservoir level of 271.6 m under five open bottom outlets. The flow rate was 430 m^3/s when the three right outlets were opened and 550 m^3/s when the two left outlets were opened. However, the scenario with three open outlets removed a larger quantity of sediments and led to a larger scour depth in the longitudinal profile. This could be attributed to the lower elevation of the three right outlets (191.3 m) than the two left ones (193.8 m).

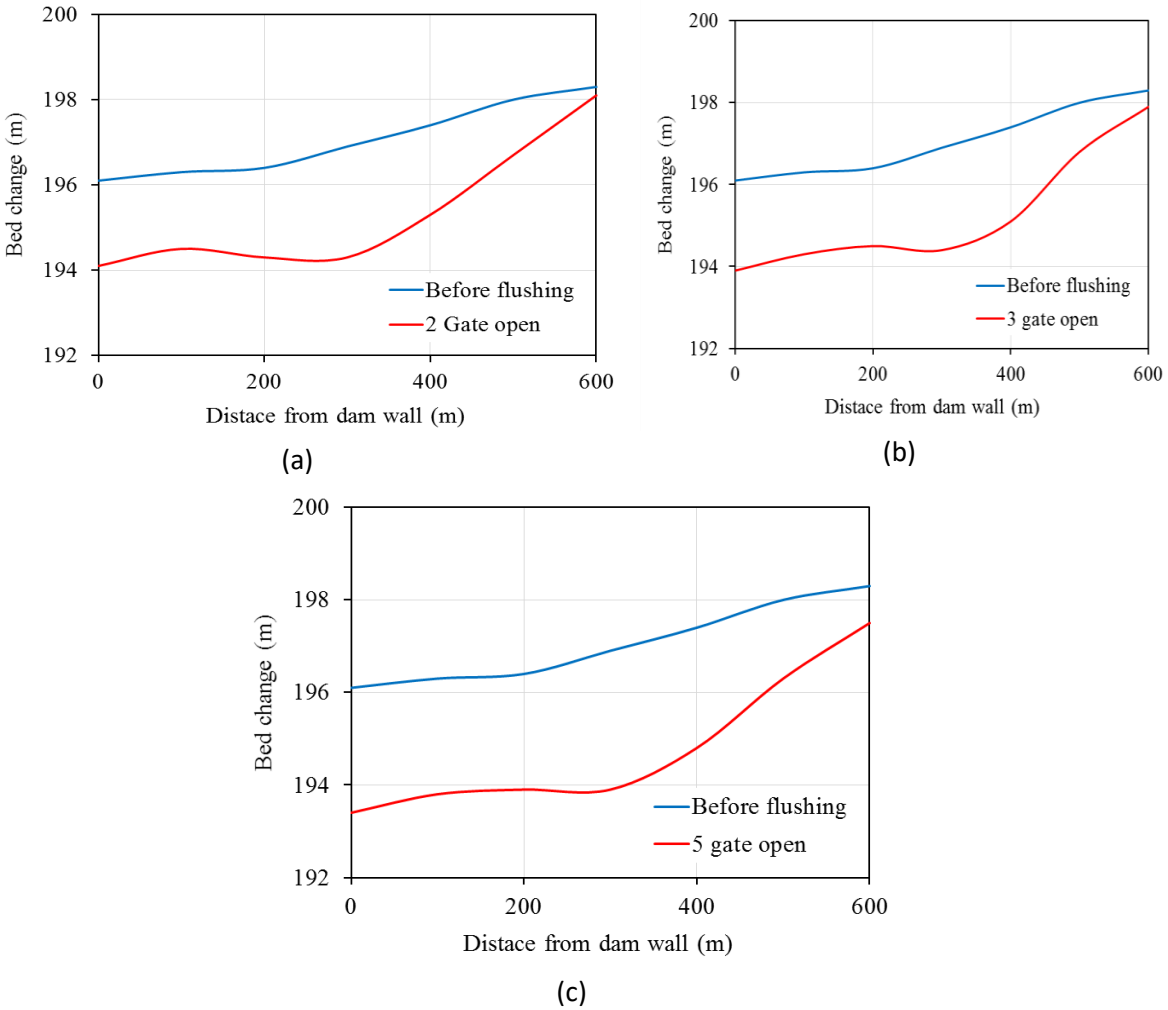

Figure 6: Bed profile change at a reservoir level of 234.6 m under (a) two, (b) three, and (c) five open outlets

ISSN：1674-2974 | CN 43-1061 / N

DOI: 10.5281/zenodo.10450360
Vol: 60 | Issue: 12 | 2023

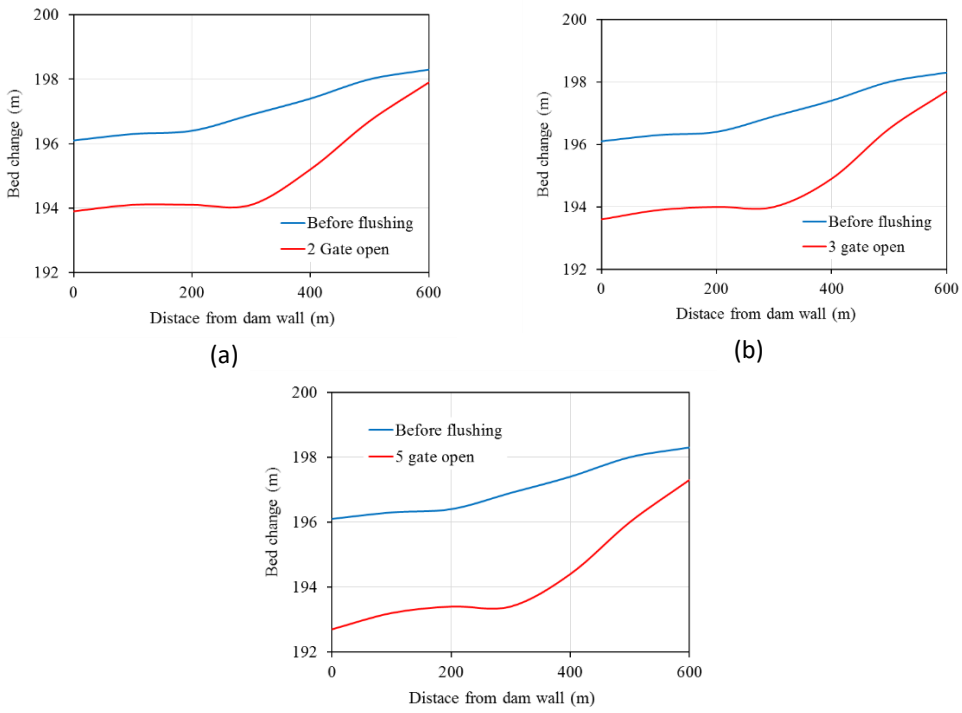

Figure 7: Bed profile change at a reservoir level of 271.6 m under (a) two, (b) three, and (c) five open outlets

Figure 8 compares the bed change at the two reservoir levels under two, three, and five open outlets. It was found that a higher initial reservoir level would lead to higher sediment removal, regardless of the number of open outlets.

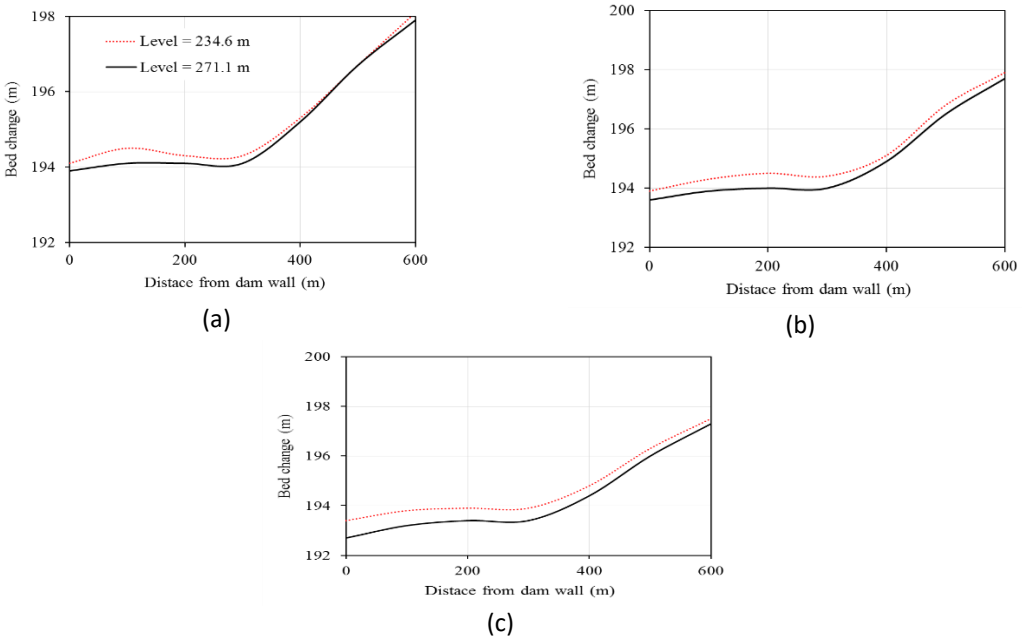

Figure 8: Bed change under (a) two, (b) three, and (c) five open outlets

ISSN：1674-2974 | CN 43-1061 / N

DOI: 10.5281/zenodo.10450360
Vol: 60 | Issue: 12 | 2023

Figure 9 compares the bed profile changes at both modeled reservoir levels under different numbers of open outlets to the 2004 flushing operation. According to Fig. 9(a), a higher initial reservoir level (271.6 m) with five open outlets had higher sediment removal than the 2004 flushing operation, while no significant difference was observed under two and three open outlets. As shown in Fig. 9(b), the numerical scenario with five open outlets showed almost the same sediment removal as the 2004 flushing operation at the same reservoir level, while the scenarios with two and three open outlets had lower sediment removal than the 2004 flushing operation.

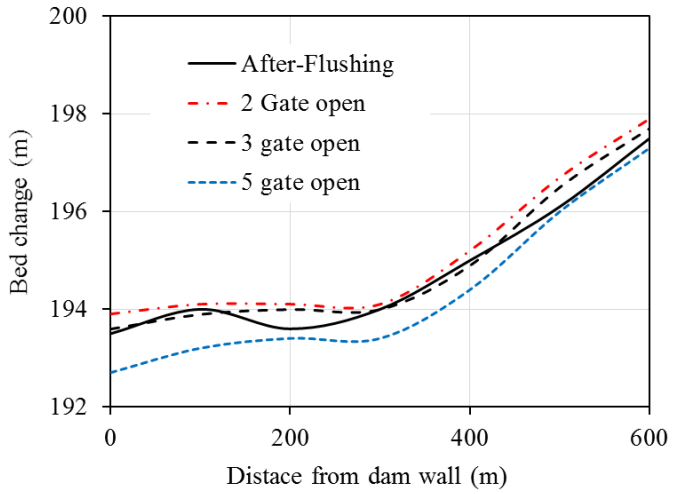

(a)

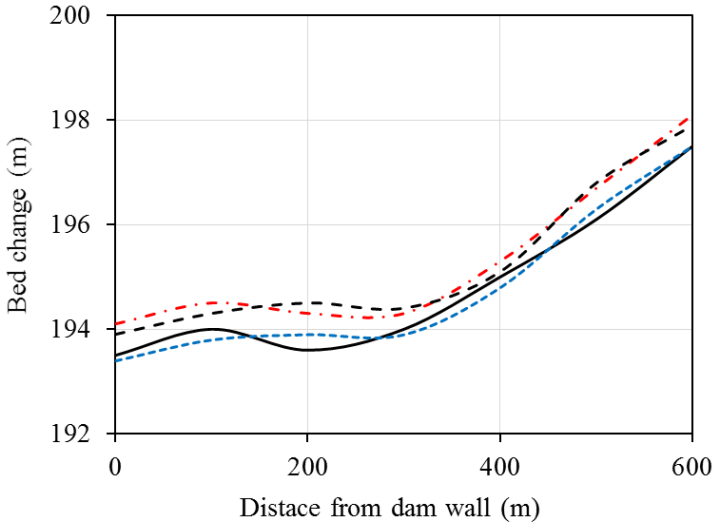

(b)

Figure 9: Bed change comparison between the 2004 flashing operation and numerical scenarios at a reservoir level of (a) 271.6 and (b) 234.6 m

Figure 10 compares the numerical flushing scenarios to the 2004 flushing operation in the bed change near the bottom outlets. As can be seen, the scenario with a reservoir level of 271.6 m and five open outlets resulted in higher removal of sediments in the vicinity of the outlets. The other scenarios with fewer open outlets showed lower erosion than the 2004 flushing operation.

ISSN：1674-2974 | CN 43-1061 / N

DOI: 10.5281/zenodo.10450360
Vol: 60 | Issue: 12 | 2023

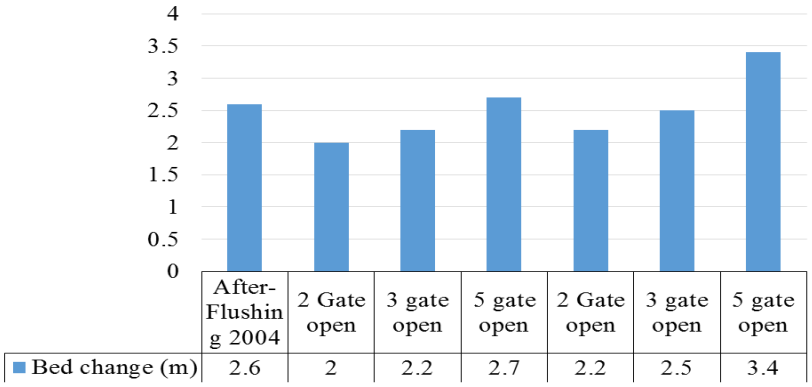

(a)

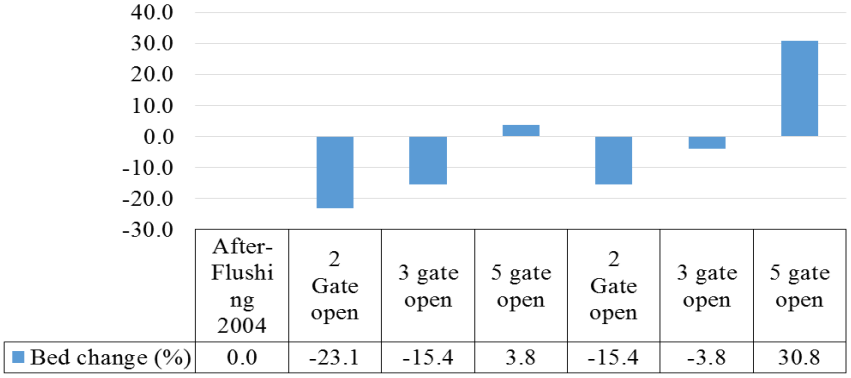

(b)

Figure 10: Comparison of the numerical scenarios and 2004 flushing operation in sediment level change near the bottom outlets

Sediment removal is a major parameter in flushing. Figure 11 plots the removed sediment quantities at different reservoir levels under different numbers of open outlets. As can be seen, a larger quantity of sediments was removed at a reservoir level of 271.6 m than at 234.6 m. Furthermore, a rise in the number of open outlets increased sediment removal. As mentioned, the normal initial reservoir level (271.6 m) and five open outlets represented the optimal scenario.

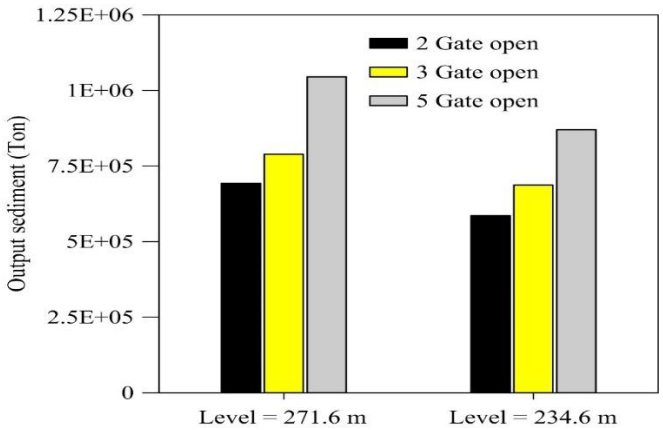

Figure 11: Total sediment removal under different scenarios

DOI: 10.5281/zenodo.10450360
Vol: 60 | Issue: 12 | 2023

CONCLUSION

The sediment management of dam reservoirs is a challenge for water resource managers and decision-makers since dams have high construction costs and significant advantages at the same time. Flushing is a common technique to diminish sediments in reservoirs. This paper evaluated the effects of the initial reservoir water level and outflow rate on sediment removal using 3D numerical simulations. The simulations were carried out at two initial reservoir water levels and different numbers of open outlets. The bed changes revealed that a rise in the initial reservoir water level led to a larger flushed area. Pressurized flushing was found to be effective at a distance of up to 600 m from the dam wall, and a rise in the distance from the wall reduced erosion. The scenario with an initial reservoir level of 271.6 m and five open outlets was found to be the optimal scenario under which nearly 1 million tons of sediments were removed. It was also found that erosion around the bottom outlets was maximized in the optimal scenario.

Data Availability Statement

All relevant data are included in the paper or its supplementary information.

Acknowledgements

The authors would like to express their gratitude to the Water Organizations of Tehran and Guilan for providing data.

References

1) Beyvazpour A., Daryaee M., & Kashefipour S.M. 2021 Improvement of pressurized flushing efficiency by installing a single pile upstream of the orifice. *Ain Shams Eng J,* **12**(1), 47–55.
2) Castillo L.G., Carrillo J.M., & Álvarez M.A. 2015 Complementary methods for determining the sedimentation and flushing in a reservoir. *Journal of Hydraulic Engineering*, **141**(11), 05015004.
3) Chaudhry M.A., Habib-ur-Rehman M., Akhtar M.N., & Hashmi H.N. 2014 Modeling sediment deposition and sediment flushing through reservoirs using 1-D numerical model. *Arab J Sci Eng,* **39**(2), 647–658.
4) Chen B. 2006 The numerical simulation of local scour in front of a vertical-wall breakwater. *Journal of Hydrodynamics*, **18**(1), 132-136.
5) Daryaee M., Ahmadi F., Peykani P., & Zayeri M. 2022 Prediction of longitudinal and transverse profiles of pressure flushing cones using artificial intelligence and data pre-processing. *Water Supply*, **22**(2), 1533-1545.
6) Emamgholizadeh S., Bateni S.M. & Jeng, D.S. 2013 Artificial intelligence-based estimation of flushing half-cone geometry. *Engineering Applications of Artificial Intelligence,* **26** (10), 2551–2558
7) Engelund F., & Fredsøe J. 1976 A sediment transport model for straight alluvial channels. *Hydrology Research,* **7**(5), 293-306.
8) Fathi-moghaddam M., Sadrabadi M.T., & Rahmanshahi M. 2018 Numerical simulation of the hydraulic performance of triangular and trapezoidal gabion weirs in free flow condition. *Flow Measurement and Instrumentation,* **62**, 93-104.
9) Flow Science Inc, Flow-3D User Manual, V11, 2015
10) Haghjouei H., Rahimpour M., Qaderi K., & Kantoush S.A. 2021 Experimental study on the effect of bottomless structure in front of a bottom outlet on a sediment flushing cone. *Int J Sedim Res,* **36**(3):335–347.
11) Haun S., & Olsen N.R.B. 2012 Three dimensional numerical modeling of the flushing process of the kali gandaki hydropower reservoir. *Lakes Reserv Res Manag* **17**(1), 25–33.
12) Iqbal M., Ghumman A.R., Haider S., Hashmi H.N., & Khan M.A. 2019 Application of Godunov type 2D model for simulating sediment flushing in a reservoir. *Arab J Sci Eng*, **44**(5), 4289–4307.

DOI: 10.5281/zenodo.10450360
Vol: 60 | Issue: 12 | 2023

13) Jenzer Althaus J.M., Cesare G.D., Schleiss A.J. 2015 Sediment evacuation from reservoirs through intakes by jet-induced flow. *J Hydraul Eng*, **141**(2), 04014078

14) Li G., Lang L., & Ning J. 2013 3D Numerical simulation of flow and local scour around a spur dike. *In IAHR World Congress* (pp. 1-9).

15) Li X., Qiu J., Shang Q. & Li F. 2016 Simulation of reservoir sediment flushing of the three gorges reservoir using an artificial neural network. *Applied Sciences* **6** (5), 148.

16) Madadi M.R., Rahimpou M., & Qaderi K. 2017 improving the pressurized flushing efficiency in reservoirs: an experimental study. *Water Resour Manage* **31**(14), 4633–4647.

17) Madadi M.R., Rahimpour M., & Qaderi K. 2016 Sediment flushing upstream of large orifices: An experimental study. *Flow Meas Instrum* **52**, 180–189.

18) Melville B. 2008 The physics of local scour at bridge piers. *In 4th International Conference on Scour and Erosion*, ICSE-4, Tokyo, Japan pp. 28–38.

19) Meshkati M.E., Dehghani A.A., Naser G., Emamgholizadeh S., & Mosaedi A. 2009 Evolution of developing flushing cone during the pressurized flushing in reservoir storage. *World Acad Sci, Eng Technol* **58**, 1107–1111.

20) Morris G.L., & Fan J. 2010 *Reservoir sedimentation handbook*. Electron version 1:04

21) Naderi S., Daryaee M., Kashefipour S.M., & Zayeri, M. 2022 Numerical and Experimental Study of Flow Pattern due to a Plate Installed Upstream of Orifice in Pressurized Flushing of Dam Reservoirs. *Iranian Journal of Science and Technology, Transactions of Civil Engineering*, 1-11.

22) Powell D.N, & Khan A.A. 2012 Scour upstream of a circular orifice under constant head. *J Hydraul Res* **50**(1), 28–34.

23) Powell D.N., & Khan A.A. 2015 Flow field upstream of an orifice under fixed bed and equilibrium scour conditions. *J Hydraul Eng 141*(2):04014076.

24) Schleiss A.J., Franca M.J., Juez C., & De Cesare G. 2016 Reservoir sedimentation. *J Hydraul Res* 54(6):595–614.

25) Shen H.W. 1999 Flushing sediment through reservoirs. *J Hydraul Res* **37**(6), 743–757.

26) Talebbeydokhti N., Naghshineh A. 2004 Flushing sediment through reservoirs. *Iranian J Sci Technol* 2**8**(B1), 119–136

27) White W.R. 2001 *Evacuation of sediment from reservoirs*, ThomasTelford, London

28) Yakhot V., & Orszag S.A. 1986 Renormalization group analysis of turbulence. I. Basic theory. *Journal of scientific computing,* **1**(1), 3-51.